

Polaritonic Chemistry using the Density Matrix Renormalization Group Method

Mikuláš Matoušek,^{1,2} Nam Vu,³ Niranjan Govind,^{4,5} Jonathan J. Foley IV,³ and Libor Veis¹

¹*J. Heyrovský Institute of Physical Chemistry, Academy of Sciences of the Czech Republic, v.v.i., Dolejškova 3, 18223 Prague 8, Czech Republic*

²*Faculty of Mathematics and Physics, Charles University, Prague, Czech Republic*

³*Department of Chemistry, University of North Carolina Charlotte, Charlotte, North Carolina 28223, United States*

⁴*Physical and Computational Sciences Directorate, Pacific Northwest National Laboratory, Richland, Washington 99352, United States*

⁵*Department of Chemistry, University of Washington, Seattle, Washington 98195, United States*

(*Electronic mail: libor.veis@jh-inst.cas.cz)

(*Electronic mail: jfoley19@charlotte.edu)

(*Electronic mail: mikulda@volny.cz)

The emerging field of polaritonic chemistry explores the behavior of molecules under strong coupling with cavity modes. Despite recent developments in *ab initio* polaritonic methods for simulating polaritonic chemistry under electronic strong coupling, their capabilities are limited, especially in cases where the molecule also features strong electronic correlation. To bridge this gap, we have developed a novel method for cavity QED calculations utilizing the Density Matrix Renormalization Group (DMRG) algorithm in conjunction with the Pauli-Fierz Hamiltonian. Our approach is applied to investigate the effect of the cavity on the S_0 - S_1 transition of n -oligoacenes, with n ranging from 2 to 5, encompassing 22 fully correlated π orbitals in the largest pentacene molecule. Our findings indicate that the influence of the cavity intensifies with larger acenes. Additionally, we demonstrate that, unlike the full determinantal representation, DMRG efficiently optimizes and eliminates excess photonic degrees of freedom, resulting in an asymptotically constant computational cost as the photonic basis increases.

I. INTRODUCTION

Photonic cavities are an excellent tool for studying the interactions between the quantised electromagnetic field and matter. Originally starting with Rydberg atoms^{1,2}, experimental developments enabled the field to move to larger systems, such as organic chromophores³. This opened a myriad of new potential applications, including polaritonic chemistry, where chemical reactions are modified through strong coupling between cavity modes and molecular electronic or vibrational degrees of freedom⁴⁻⁷. These developments go hand in hand with the need for accurate theoretical methods, allowing us to be confident in both our predictive abilities and the interpretation of experimental results⁸.

A detailed understanding of molecular structure and dynamics when cavity modes strongly couple to molecular electronic degrees of freedom (i.e. electronic strong coupling) requires that both electronic and photonic degrees of freedom are treated on equal quantum mechanical footing. One route that has been pursued by several groups recently includes generalizing the tools of *ab initio* electronic structure theory to explicitly include coupling to quantized photonic degrees of freedom. Such approaches have included quantum electrodynamics generalizations of density functional theory (QEDFT⁹⁻¹⁵ and QED-DFT¹⁶⁻¹⁸), real-time^{9,10,19-22} and linear-response^{16,23,24} formulations of QED-TDDFT, configuration interaction (QED-CIS)^{25,26}, cavity QED extension of second-order Møller-Plesset perturbation theory and the algebraic diagrammatic construction^{27,28}, coupled cluster (QED-CC)^{18,29-31}, variational QED-2-RDM methods³², and diffusion quantum Monte Carlo (QMC)³³. Many of the afore-

mentioned methods, however, cannot properly describe strong (multireference) electronic correlation present in many interesting molecular systems, such as transition metal complexes. The recently-reported QED-CASCI approach²⁶ and QED-2-RDM methods are well suited for describing strong correlation, but both have important limitations. QED-2-RDM methods have polynomial scaling with respect to the active space size, but so far, these variational approaches are designed to simulate the lowest energy states of a given spin symmetry, which are of limited utility for studying polariton states³². The QED-CASCI method can be used to compute multiple states, but scales exponentially with the active space size, putting a hard limit of less than 20 correlated orbitals²⁶. The exponential scaling of CASCI is usually surpassed by using approximations to such as Selected-CI³⁴⁻³⁶, heat-bath CI³⁷, full-CI QMC³⁸, or DMRG³⁹⁻⁴¹. To this end, we present a QED extension to the Density Matrix Renormalization Group method (QED-DMRG) that can provide efficient controlled approximations to numerically-exact solutions to the Pauli-Fierz Hamiltonian¹⁵. QED-DMRG also provides a powerful representation for approximating multiconfigurational multi-component wavefunctions with similar accuracy and significantly lower computational cost than the recently-reported QED-CASCI approach.

In what follows, we briefly review the basics of the DMRG method and outline the extensions necessary for QED-DMRG. Since our DMRG implementation (MOLMPS program⁴²) employs the renormalized operators rather than the matrix product operators (MPOs), the presentation follows the original renormalization group picture⁴³. In order to demonstrate the accuracy of QED-DMRG, we present its

application on the eigenstates of the Pauli-Fierz (PF) Hamiltonian tuned to the excitation from the ground to the first excited singlet state (S_0 to S_1) of n -oligoacenes with $n \in (2, 5)$. For a discussion on the excited states of n -oligoacenes using a broad spectrum of excited-state theoretical approaches, we refer the reader to Ref. 44 and references therein.

II. THEORY

A. Quantum chemical DMRG method

While the Density Matrix Renormalization Group (DMRG) method has origins in solid state physics^{43,45}, it is already established also in the realm of quantum chemistry³⁹⁻⁴¹, sometimes abbreviated as QC-DMRG. Here the DMRG algorithm is used to find the eigenstates of the electronic Hamiltonian

$$H_{\text{el.}} = \sum_{\sigma} \sum_{pq} h_{pq} a_{p\sigma}^{\dagger} a_{q\sigma} + \frac{1}{2} \sum_{\sigma\sigma'} \sum_{pqrs} \langle pq|rs \rangle a_{p\sigma}^{\dagger} a_{q\sigma'}^{\dagger} a_{s\sigma'} a_{r\sigma}, \quad (1)$$

where h_{ij} and $\langle ij|kl \rangle$ denote standard one and two-electron integrals in the restricted molecular orbital (MO) basis, and σ and σ' denote spin, $\sigma, \sigma' \in \{\uparrow, \downarrow\}$.

The DMRG method is based on the Matrix Product State (MPS)⁴⁶ wave function ansatz, in which the exact FCI wave function (in the occupation basis representation)

$$|\Psi_{\text{FCI}}\rangle = \sum_{n_1 \dots n_k} c^{n_1 n_2 \dots n_k} |n_1 n_2 \dots n_k\rangle \quad (2)$$

is factorized into a linear tensor network

$$|\Psi_{\text{MPS}}\rangle = \sum_{n_1 \dots n_k} \sum_{i_1 \dots i_{k-1}} A[1]_{i_1}^{n_1} A[2]_{i_1 i_2}^{n_2} \dots A[k]_{i_{k-1}}^{n_k} |n_1 \dots n_k\rangle. \quad (3)$$

The tensors $A[j]$ have three indices. One physical, here labeled n_j , corresponding to a physical degree of freedom. In quantum chemistry these are the possible occupations of a single molecular orbital ($|\cdot\rangle, |\uparrow\rangle, |\downarrow\rangle, |\uparrow\downarrow\rangle$), leading to a dimension of four. The other two (i_{j-1}, i_j) are called virtual, and they are contracted with the neighboring tensors. The dimension of these indices, called the bond dimension, is the main parameter controlling both the accuracy and the computational cost⁴⁰. Since the bond dimension is in practical approximate calculations bounded, the number of DMRG variational parameters is, in contrast to FCI, polynomial.

The optimization of the individual tensors in the network is then performed sequentially in a process called sweeping. The standard two-site algorithm is based on the separation of the tensor network into four parts, the two sites taken explicitly ($j, j+1$), all the sites to the left of the explicit sites ($i < j$, so called left block) and the sites on the right ($i > j+1$, right block). It provides the wave function in the two-site MPS form⁴⁶

$$|\Psi_{2\text{-site-MPS}}\rangle = \sum_{\{n\}} \sum_{\{i\}} A_{i_1}^{n_1} \dots A_{i_{j-2} i_{j-1}}^{n_{j-1}} \Psi_{i_{j-1} i_{j+1}}^{n_j n_{j+1}} A_{i_{j+1} i_{j+2}}^{n_{j+2}} \dots A_{i_{k-1}}^{n_k} |n_1 \dots n_k\rangle, \quad (4)$$

where we have for simplicity omitted the MPS tensor square brackets with the site indices. The uncontracted virtual indices on the left and right blocks form the orthonormal many-particle bases ($\{|l\rangle\}, \{|r\rangle\}$), which span a subspace of the full Hilbert space of a given block. The orthonormality stems from the fact that the MPS tensors formed during the DMRG sweeping via the singular value decomposition (SVD, see below) fulfil the following conditions

$$\sum_{n_j} (\mathbf{A}[j]^{n_j})^{\dagger} \mathbf{A}[j]^{n_j} = \mathbf{I} \quad j \in \text{left} \quad (5)$$

$$\sum_{n_j} \mathbf{A}[j]^{n_j} (\mathbf{A}[j]^{n_j})^{\dagger} = \mathbf{I} \quad j \in \text{right} \quad (6)$$

The four-index tensor $\Psi_{i_{j-1} i_{j+1}}^{n_j n_{j+1}}$ in Eq. 4 is in each iteration of the sweeping procedure obtained by solving the Schrödinger equation projected onto the product space of the left block, two explicit sites, and the right block. The effective equation has, due to the orthonormality of the left and right block bases mentioned above, a form of a standard eigenvalue problem

$$H_{\text{el.}} |\Psi\rangle = E |\Psi\rangle, \quad (7)$$

which is solved by means of iterative solvers such as the Davidson algorithm⁴⁷. The wave function is expanded as

$$|\Psi\rangle = \sum_{l, n_j, r} \Psi_{lr}^{n_j n_{j+1}} |l\rangle \otimes |n_j\rangle \otimes |n_{j+1}\rangle \otimes |r\rangle. \quad (8)$$

Notice that $|l\rangle$ labels basis states of the left block, which contains $j-1$ sites, i.e. they correspond to the aforementioned uncontracted MPS virtual index i_{j-1} .

$$|l\rangle \equiv |\psi_{i_{j-1}}\rangle = \sum_{n_1 \dots n_{j-1}} \sum_{i_1 \dots i_{j-2}} A_{i_1}^{n_1} A_{i_1 i_2}^{n_2} \dots A_{i_{j-2} i_{j-1}}^{n_{j-1}} |n_1 \dots n_{j-1}\rangle. \quad (9)$$

Similarly $|r\rangle$ corresponds to the uncontracted virtual index i_{j+1} .

In DMRG, the explicit (determinant) representations of the complicated many-particle bases ($\{|l\rangle\}, \{|r\rangle\}$) are not stored, because it would lead to the original exponential scaling. Instead, the matrix representations of second-quantized operators needed for the action of the Hamiltonian on a wave function (see Eq. 7) are formed and stored. The matrix representations of a single site annihilation operators (in the $\{|\cdot\rangle, |\uparrow\rangle, |\downarrow\rangle, |\uparrow\downarrow\rangle\}$ basis) read

$$a_{\uparrow} = \begin{pmatrix} 0 & 0 & 1 & 0 \\ 0 & 0 & 0 & 1 \\ 0 & 0 & 0 & 0 \\ 0 & 0 & 0 & 0 \end{pmatrix}, \quad a_{\downarrow} = \begin{pmatrix} 0 & 1 & 0 & 0 \\ 0 & 0 & 0 & 0 \\ 0 & 0 & 0 & -1 \\ 0 & 0 & 0 & 0 \end{pmatrix}. \quad (10)$$

When working with the enlarged left block (L) as a tensor product of the left block states with the states on the explicit

left site and similarly the right enlarged block (R), the Hamiltonian for this bipartite splitting reads

$$H_{\text{el.}} = H_L \otimes I_R + I_L \otimes H_R + \sum_{\alpha} H_L^{\alpha} \otimes H_R^{\alpha}, \quad (11)$$

where $H_{L/R}$ represent the enlarged left/right block Hamiltonians, i.e. all indices in Eq. 1 belonging to the corresponding blocks and the last summation term represents the interaction between enlarged left and right blocks with indices split between both blocks. Let us demonstrate the main strategies on the example of the simpler one-electron Hamiltonian

$$H_{\text{one-el.}} = \sum_{pq} h_{pq} a_{p\uparrow}^{\dagger} a_{a\uparrow} + \sum_{pq} h_{pq} a_{p\downarrow}^{\dagger} a_{a\downarrow}. \quad (12)$$

Here, the interaction between the enlarged blocks consists of the two contributions

$$\begin{aligned} H_{\text{one-el.}}^{\text{int}} &= \sum_{q \in R} \left\{ \sum_{p \in L} h_{pq} a_{p\uparrow}^{\dagger} \right\}_L \otimes (a_{q\uparrow})_R \\ &+ \sum_{q \in R} \left\{ \sum_{p \in L} h_{pq} a_{p\downarrow}^{\dagger} \right\}_L \otimes (a_{q\downarrow})_R \\ &- \text{h. c.} \end{aligned} \quad (13)$$

In order to reduce the number of matrix-matrix multiplications during the action of the Hamiltonian on a wave function, which are the most CPU-demanding tasks, the efficient QC-DMRG codes work with the so called presumed (or partially summed) operators⁴⁸, i.e. intermediates formed by contraction of operator matrices with MO integrals. In case of the one-electron Hamiltonian, Eq. 13, the enlarged left block one-electron presumed operators are encapsulated in the curly brackets and are defined as

$$A_q^{\uparrow} = \sum_{p \in L} h_{pq} a_{p\uparrow}^{\dagger}, \quad q \notin L \quad (14)$$

$$A_q^{\downarrow} = \sum_{p \in L} h_{pq} a_{p\downarrow}^{\dagger}, \quad q \notin L \quad (15)$$

The interaction terms are always composed of presumed operators on the one block and normal operators on the other block. In the case of one-electron Hamiltonian (13)

$$H_{\text{one-el.}}^{\text{int}} = \sum_{q \in R} (A_q^{\uparrow})_L \otimes (a_{q\uparrow})_R + \sum_{q \in R} (A_q^{\downarrow})_L \otimes (a_{q\downarrow})_R - \text{h.c.} \quad (16)$$

Since the presumed operators are for efficiency reasons formed on the longer block, a switching between normal and presumed operators has to be done in the middle of each sweep.

The transition from one iteration of the sweep to another is carried out by means of the renormalization procedure. In this step, the basis of one of the blocks is, in the direction of the

sweep, enlarged by one new site and the operators needed for the action of the Hamiltonian on the trial wave function are transformed into the new basis. The complementary block is, on the other hand, reduced by one site. This effectively moves us by one tensor in the MPS and the diagonalization of the effective Hamiltonian (Eq. 7) can be repeated. The exact basis obtained by enlarging by one site would be a tensor product between the original basis and the basis of the new site. This is unacceptable, as the size of the new basis would be a product of the sizes of the old basis and the basis of the added site. The choice of truncation of the new basis gave the name to the method, the basis is truncated so that the density matrix of the new block is changed as little as possible. This is done by diagonalizing the density matrix and keeping only the largest eigenvalues. When the wave function expansion coefficients $\Psi_{l_r}^{n_j n_{j+1}}$ (8) are reshaped into the matrix form $\Psi_{(ln_j), (n_{j+1}r)}$, the aforementioned reduced density matrices can be computed in the following way

$$\rho^L = \Psi \Psi^{\dagger}, \quad (17)$$

$$\rho^R = \Psi^{\dagger} \Psi. \quad (18)$$

For the transition to the next iteration, all operator matrices formed for the enlarged block have to be renormalized

$$\mathbf{A}' = (\mathbf{O}^L)^{\dagger} \mathbf{A} \mathbf{O}^L, \quad (19)$$

where \mathbf{A} represents an operator matrix in the non-truncated ($4M$ -dimensional) basis and \mathbf{A}' is the renormalized matrix representation in the truncated (M -dimensional) basis.

The procedure outlined above effectively performs an SVD decomposition on the wave function (8)

$$\Psi_{i_{j-1}i_{j+1}}^{n_j n_{j+1}} \xrightarrow{\text{SVD}} A_{i_{j-1}i_j}^{n_j} M_{i_j i_{j+1}}^{n_{j+1}}, \quad (20)$$

where the new MPS tensor $A[j]$ is formed and the three-leg tensor $M[j+1]$ represents the rest of the SVD factorization. SVD in fact produces the best approximation of bipartite wave functions⁴⁶. The sum of the discarded eigenvalues is then called the Truncation Error (TRE).

B. Cavity QED-DMRG method

The generalization of DMRG to multiple particle types is straightforward. The Hamiltonian now contains a mix of creation and annihilation operators corresponding to the different particle types, which separately satisfy own commutation/anti-commutation rules. Each of the particle types is assigned its own set of sites in the MPS wave function and renormalized operators for all particle types, including the mixed terms describing the interaction between models, have to be formed. Previously, the QC-DMRG method has been generalized for the beyond-Born-Oppenheimer nuclear-electronic all-particle (NEAP) calculations^{49,50} and applied

on the proton-electron problems, i.e. spin- $\frac{1}{2}$ fermionic interactions. Herein, we generalize the QC-DMRG method for applications in polaritonic chemistry in which electronic (fermionic) and photonic (bosonic) degrees of freedom are treated on equal footing. Below, we give the details specific to this generalization.

We will restrict ourselves to the Pauli-Fierz (PF) Hamiltonian within the dipole approximation, which describes coupling of molecular systems to a single cavity (photonic) mode

$$H_{\text{PF}} = H_{\text{el.}} + \omega b^\dagger b - \sqrt{\frac{\omega}{2}} \boldsymbol{\lambda} \cdot \boldsymbol{\mu} (b^\dagger + b) + \frac{1}{2} (\boldsymbol{\lambda} \cdot \boldsymbol{\mu})^2, \quad (21)$$

where $H_{\text{el.}}$ is the electronic Hamiltonian (1), ω is the cavity photon frequency, $\boldsymbol{\mu}$ represents the molecular dipole operator, $\boldsymbol{\lambda}$ is a coupling vector, and b^\dagger , b denote photonic creation and annihilation operators. The second term in Eq. 21 corresponds to the harmonic oscillator Hamiltonian of the bare cavity mode, the third term represents the so called bilinear coupling, and the last one is the dipole self-energy term. We will assume the Cartesian coordinate system, thus $\boldsymbol{\lambda}$ and $\boldsymbol{\mu}$ have x , y , and z components. It is convenient to define the scalar molecular dipole coupling operator as $d = \boldsymbol{\lambda} \cdot \boldsymbol{\mu}$.

Following the previous work on QED-CASCI²⁶, we compare two approaches differing by the input molecular orbitals. The simpler scenario corresponds to using the standard Hartree-Fock (HF) orbitals and searching for the eigenstates of the PF Hamiltonian presented in Eq. 21. In this case and similarly to Eq. 2, the QED-FCI wave function is expanded in the so called particle number (PN) basis

$$|\Psi_{\text{QED-FCI}}\rangle = \sum_N \sum_{n_1 \dots n_k} c^{N n_1 n_2 \dots n_k} |N^{\text{ph.}}\rangle \otimes |n_1 n_2 \dots n_k^{\text{el.}}\rangle, \quad (22)$$

where $|N^{\text{ph.}}\rangle$ denotes the photonic PN basis, which comprises states $|0\rangle, |1\rangle, |2\rangle, \dots, |n_{\text{max}}\rangle$, n_{max} being the maximum photon occupation.

The second strategy is to perform the QED-HF calculation and transform from the PN basis into the coherent state (CS) basis^{51,52} by means of the unitary transformation

$$U_{\text{CS}} = \exp(z(b^\dagger - b)), \quad z = \frac{-\langle \boldsymbol{\mu}_{\text{QED-HF}} \rangle \cdot \boldsymbol{\lambda}}{\sqrt{2\omega}}. \quad (23)$$

In order to keep the same wave function expansion as in Eq. 22, U_{CS} is applied at the level of the Hamiltonian (21), which yields the PF Hamiltonian in the coherent state basis

$$H_{\text{CS}} = H_{\text{el.}} + \omega b^\dagger b - \sqrt{\frac{\omega}{2}} (d_e - \langle d_e \rangle) (b + b^\dagger) + \frac{1}{2} (d_e - \langle d_e \rangle)^2, \quad (24)$$

where denoted as d_e and $\langle d_e \rangle$ we keep only the electronic part of the dipole coupling operator d and of the coupling expectation value $\langle d \rangle = \langle \boldsymbol{\mu}_{\text{QED-HF}} \rangle \cdot \boldsymbol{\lambda}$, because the nuclear parts cancel under the Born-Oppenheimer approximation.

We would like to point out that the reference state $|0^{\text{ph.}}\rangle \otimes |\phi_0^{\text{el.}}\rangle$ transformed into the CS basis formally includes an infinite number of photon occupation states, due to the exponential form of U_{CS} ²⁶. Consequently, it was shown to outperform the PN basis in the correlated QED-CASCI calculations²⁶.

C. Implementation details

In adapting QC-DMRG for the PF Hamiltonian, the electronic part is identical to QC-DMRG, but we include a single photonic site. Herein, we have restricted ourselves to a single cavity mode, but the Hamiltonian (21), can be easily generalized for multiple cavity modes²⁵ and generalization of the implementation described below is straightforward. Note that the dimension of the photonic site is not 4 as in the case of the electronic sites, but arbitrary, corresponding to the maximum number of photons included in the wave function.

In our cavity QED-DMRG implementation, we place the photonic site as the leftmost site in the chain. The advantage is twofold. First, at any point over the sweep, the photonic operators are only in the left block. As a result, the rules for the combination of the operators on different blocks to form the Hamiltonian remain unchanged along the sweep. The second advantage is that the right block operators are identical to the QC-DMRG case and we can use the standard CI-DEAS warm-up procedure⁵³ for the generation of electronic operators in the first sweep. We would like to note that a similar idea of using a single higher dimensional electronic site was used previously^{54,55} albeit in a different context.

The single-site matrix representation of the bosonic annihilation operator b in the basis $\{|0\rangle, |1\rangle, |2\rangle, \dots, |n_{\text{max}}\rangle\}$, analogously to Eq. 10, has the matrix representation

$$b = \begin{pmatrix} 0 & \sqrt{1} & 0 & 0 & & & & & & & \\ 0 & 0 & \sqrt{2} & 0 & & & & & & & \\ 0 & 0 & 0 & \sqrt{3} & & & & & & & \\ 0 & 0 & 0 & 0 & \sqrt{4} & & & & & & \\ & & & & & \ddots & \ddots & & & & \\ & & & & & & & 0 & \sqrt{n_{\text{max}}} & & \\ & & & & & & & 0 & 0 & & \end{pmatrix} \quad (25)$$

and the creation operator b^\dagger is its hermitian conjugate.

To derive the working form of the PF Hamiltonian, we group the terms containing creation and annihilation operators of only electrons, electrons and photons, and only photons. Here, we present this approach for the CS basis formulation (24). The corresponding PN basis formulation can be readily obtained with a few substitutions in the integrals.

The H_{CS} Hamiltonian can be rewritten as

$$H_{\text{CS}} = H'_{\text{el.}} - \sqrt{\frac{\omega}{2}} \sum_{\sigma} \sum_{pq} d_{pq} a_{p\sigma}^\dagger a_{q\sigma} (b + b^\dagger) + \omega b^\dagger b + \sqrt{\frac{\omega}{2}} \langle d_e \rangle (b + b^\dagger) + \frac{1}{2} \langle d_e \rangle^2, \quad (26)$$

where the modified electronic Hamiltonian has the same two-body structure as in Eq. 1, but with the following MO integrals

$$\langle pq|rs\rangle' = \langle pq|rs\rangle + d_{pr}d_{qs}, \quad (27)$$

$$h_{pq}' = h_{pq} - \langle d_e \rangle d_{pq} - \frac{1}{2}q_{pq} \quad (28)$$

and d_{pq} and q_{pq} represent modified electric dipole and electric quadrupole integrals given by

$$d_{pq} = - \sum_{a \in \{x,y,z\}} \lambda_a \int \phi_p^*(\mathbf{r}) r_a \phi_q(\mathbf{r}) d\mathbf{r}, \quad (29)$$

$$q_{pq} = - \sum_{a,b \in \{x,y,z\}} \lambda_a \lambda_b \int \phi_p^*(\mathbf{r}) r_a r_b \phi_q(\mathbf{r}) d\mathbf{r}. \quad (30)$$

As was mentioned above, only the left block carries the photonic operators, therefore the rules for building the action of the Hamiltonian on a trial wave function when employing the bipartite enlarged L-R splitting do not change along the DMRG sweep. The purely photonic operators (third and fourth terms in Eq. 26) can be added/absorbed into the left block Hamiltonian, which is coupled with an identity operator on the enlarged right block.

The second term in Eq. 26) needs to be separated into several contributions with a different number of operators acting on the right block

$$\begin{aligned} & \left\{ -\sqrt{\frac{\omega}{2}} \sum_{\sigma} \sum_{p,q \in L} d_{pq} a_{p\sigma}^{\dagger} a_{q\sigma} (b + b^{\dagger}) \right\}_L \otimes (\text{id})_R, \\ & \sum_{\sigma} \sum_{q \in R} \left\{ -\sqrt{\frac{\omega}{2}} \sum_{p \in L} d_{pq} a_{p\sigma}^{\dagger} (b + b^{\dagger}) \right\}_L \otimes (a_{q\sigma})_R - \text{h.c.}, \\ & \sum_{\sigma} \sum_{p,q \in R} \left\{ -\sqrt{\frac{\omega}{2}} d_{pq} (b + b^{\dagger}) \right\}_L \otimes (a_{p\sigma}^{\dagger} a_{q\sigma})_R. \end{aligned} \quad (31)$$

In our pilot implementation, we do not switch between the normal and presumed operators in the middle of each sweep, but perform presumptions only on the left block. This way, we can absorb the first contribution from Eq. 31 into the left block Hamiltonian. The left block part of the second contribution is then absorbed into A_q^{\uparrow} and A_q^{\downarrow} operators (14, 15), which are combined with a single annihilation operator on the enlarged right block. Similarly, the left block part of the third contribution can be absorbed into the presumed quadratic operators, which are coupled with quadratic operators on the enlarged right block.

Another thing to note is that while the number of electrons needs to be kept fixed throughout the calculation, and forces us to keep track of the number of electrons and spin quantum numbers in each of the renormalized states, no such thing is necessary for the number of photons, as generally the wave function will contain contributions from states with different numbers of photons, and also the renormalized states will mix the number of photons together. This is in stark contrast to

works combining bosonic degrees of freedom with quantum chemical DMRG for non-Born-Oppenheimer calculations⁵⁶, which preserve the number of bosonic particles. In solid state physics, however, the Hubbard Holstein model is used, which does not preserve the number of phonons⁵⁷⁻⁶⁰.

III. COMPUTATIONAL DETAILS

To demonstrate the performance of the cavity QED-DMRG method, we performed all- π calculations of n -oligoacenes with n ranging from 2 to 5, i.e. naphthalene, anthracene, tetracene, and pentacene. The geometries used were optimized (similarly to ref. 61) at the UB3LYP/6-31G(d,p) level. For all subsequent calculations we used the cc-pVDZ basis set.⁶² Naphthalene, which was recently analyzed using the QED-CASCI method²⁶, served as a basis for establishing the convergence of QED-DMRG with QED-CASCI results. For higher acenes, we investigate how the results, particularly the energy gap between polaritonic states, scale with the number of aromatic rings.

The performance of QC-DMRG is well known to depend heavily on the type of orbitals used and their ordering on the 1D lattice⁶³. To investigate the effect of orbital type on QED-DMRG, we compared the performance of two different sets of spatial orbitals. In addition to canonical orbitals, we employed Pipek-Mezey split-localized orbitals. The ordering of the orbitals was optimized using the Fiedler algorithm,⁶⁴⁻⁶⁶ based solely on the purely electronic part of the Hamiltonian. Due to our implementation, the photon site was fixed as the leftmost site in the chain.

Furthermore, we compared two different formulations of the PF-Hamiltonian presented in Section II B, namely the CS formulation (24) and the PN formulation (21). It is worth noting that in the case of QED-CASCI, the CS formulation was shown to perform better²⁶. The two-site DMRG calculations were initialized using the CI-DEAS warm-up procedure⁵³ and employed either fixed bond dimensions or variable bond dimensions, achieving the predefined truncation error through the Dynamical Block State Selection (DBSS) approach⁶⁷.

As mentioned above, the comparison with QED-CASCI has been done on the naphthalene molecule, with the photon energy tuned to S_0 - S_1 transition energy of $0.160984 E_h$. We used a coupling vector oriented in plane along the short axis of the molecule. The size of the coupling varied from 0.005 to 0.2 atomic units (a.u.).

Similarly for the larger acenes, where we only studied the behavior of the different states with the coupling strength, we used the photon energy equal to the S_0 - S_1 transition at the zero coupling strength calculated with DMRG. This gave us an excitation energy of $0.14083 E_h$ for anthracene, $0.12741 E_h$ for tetracene and $0.11840 E_h$ for pentacene. We used a fixed bond dimension $M = 1000$. We compared two different orientations of the coupling vector, along the short axis of the molecule and along the long axis.

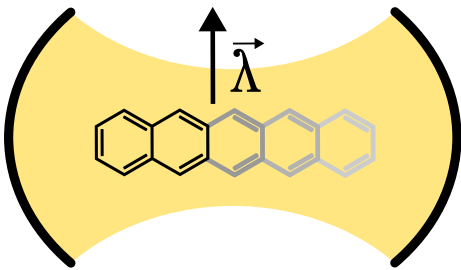


FIG. 1: Orientation along the short axis of the oligoacene series, used throughout the majority of the calculations.

IV. RESULTS AND DISCUSSION

Let's begin by comparing QED-DMRG and QED-CASCI on the naphthalene molecule. Figure 2 illustrates the energetic error of QED-DMRG relative to QED-CASCI for the lower polaritonic state across three different coupling strengths. Increasing the bond dimension allows us to reduce the error below our convergence threshold of $10^{-6} E_h$ for DMRG. The almost linear dependence in a semi-logarithmic plot hints at a roughly exponential decrease of the error with an increasing bond dimension^{39,68,69}. One can observe that with increasing coupling strength, the error for a given bond dimension grows due to greater entanglement between photonic and electronic degrees of freedom.

Similarly to QC-DMRG, we can see in Figure 2 that the truncation error is strongly reduced by localization of the active orbitals, the truncation error being an order of magnitude lower with the same bond dimension. Thus, for calculations of higher acenes, we have employed the split-localized orbitals. Overall, we found that for naphthalene with a split-localized basis we can achieve submiliHartree accuracy with respect to QED-CASCI quite easily, even with a rather small bond dimension of 256.

In Table I we show the truncation error and the RMSD of the five lowest states with respect to the reference CASCI depending on the magnitude of the cavity coupling. Similarly as with the error in energy, the truncation error grows with increasing the coupling strength. However, the growth is not very dramatic, with less than a 20% increase of the TRE with an order of magnitude stronger coupling.

Figure 3 shows the dependence of the energy error on the TRE set for various coupling strengths. A linear trend is observed for small TRE values, similar to QC-DMRG, which enables extrapolation of the energy to a zero TRE limit, which should in theory be equivalent to the exact CASCI energy. The errors of the extrapolated energies are $-1 \cdot 10^{-6}$, $-1 \cdot 10^{-6}$, and $9 \cdot 10^{-6}$ atomic units for coupling values of $|\lambda| = 0.005$ a.u., $|\lambda| = 0.05$ a.u., and $|\lambda| = 0.2$ a.u., respectively. These errors are significantly lower than those of the most accurate calculations used for the extrapolation, which had a TRE of $1 \cdot 10^{-6}$.

In Figure 4 we show the error in energy of the polaritonic state of naphthalene with respect to the maximum number of photons in the wave function. The error is calculated for the coupling strength $\lambda = 0.2$ a.u. as a difference between the

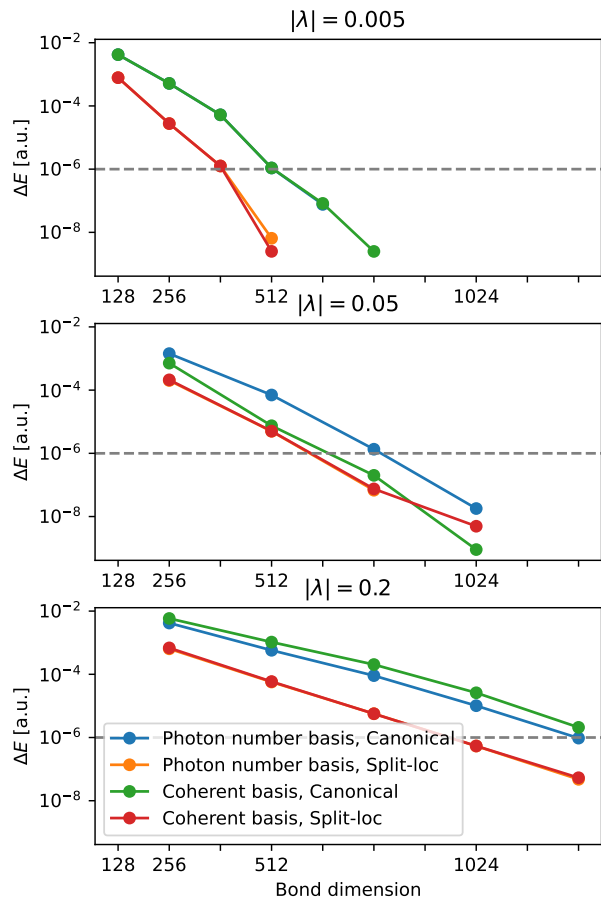


FIG. 2: Comparison of the energetic errors in QED-DMRG with respect to exact QED-CASCI for the lower polaritonic state of naphthalene, using PN and CS Hamiltonian formulations in both canonical and split-localized MO bases. Results are shown for varying bond dimensions and three coupling strengths. The orange and red curves overlap in all three plots.

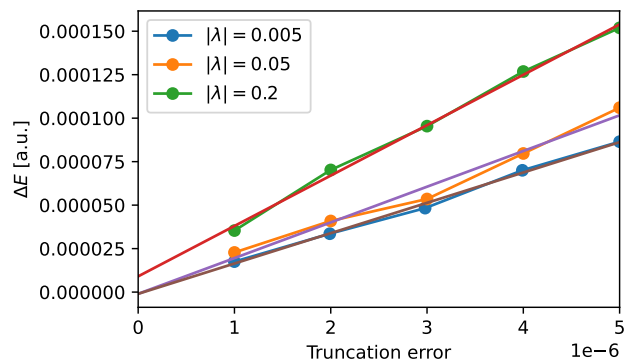


FIG. 3: Dependence of the error in energy with the truncation error for the polaritonic state of naphthalene with different coupling strengths

TABLE I: Truncation error of naphthalene with a bond dimension of 256 for different values of the coupling strength and the root mean square deviation (RMSD) of energies of the 5 lowest states from the exact CASCI energy.

Lambda (a.u.)	0	0.005	0.01	0.02	0.03	0.04	0.05
Can-TRE	2.12E-03	2.12E-03	2.17E-03	2.21E-03	2.26E-03	2.35E-03	2.45E-03
Loc-TRE	7.28E-05	1.49E-04	1.51E-04	1.52E-04	1.60E-04	1.68E-04	1.77E-04
Can-RMSD	5.71E-04	5.64E-04	5.63E-04	6.34E-04	6.87E-04	7.51E-04	8.21E-04
Loc-RMSD	2.60E-08	7.12E-05	7.37E-05	8.02E-05	9.10E-05	9.65E-05	1.04E-04

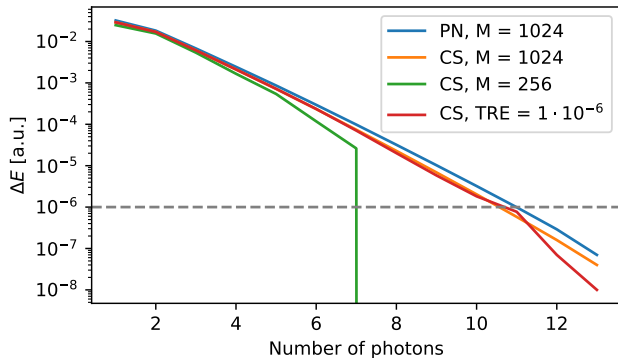


FIG. 4: Energy difference between the polaritonic state with a given number of photons and the converged state with 14 photons, illustrating the saturation of the naphthalene wave function with photons. PN denotes the particle number basis, and CS denotes the coherent state basis.

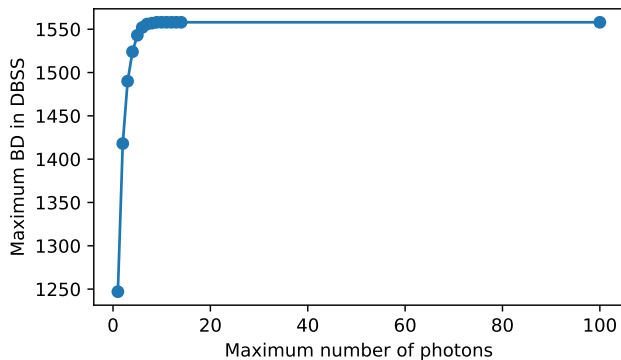


FIG. 5: Maximum bond dimension required for a given maximum number of photons, illustrating the renormalization of unnecessary degrees of freedom. The analysis is based on naphthalene with a coupling strength of 0.2 and a target truncation error (TRE) of 10^{-6} .

energy with a given number of photons and the energy with 14 photons, which we considered converged. We can observe that the error decreases roughly exponentially with the number of photons, similar to ref. 26. Nevertheless, the approximate nature of DMRG introduces additional features worth discussing. Using a bond dimension of 1024, which yields energies almost identical to the reference CASCI, we observe

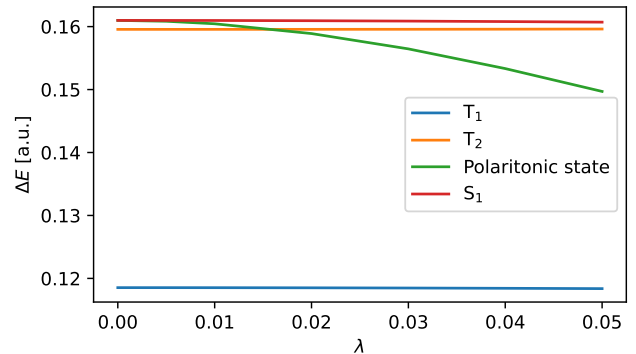


FIG. 6: Energy differences between the ground state and excited states of the naphthalene molecule at a given coupling strength.

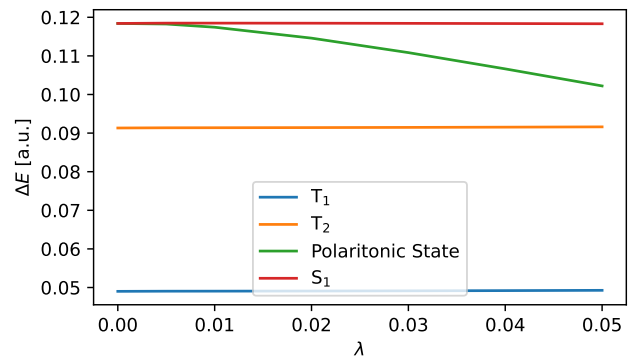


FIG. 7: Energy differences between the ground state and excited states of the pentacene molecule at a given coupling strength.

proper scaling across the entire range of values. Conversely, reducing the bond dimension to 256 limits the flexibility of the wave function, making it unable to fully account for the number of photons. As such, the system artificially gets saturated with a much smaller number of photons. Increasing the number of photons beyond this saturation limit results in nearly no changes to the resulting wave function and the change in energy abruptly drops to zero. Similarly, with DBSS the resulting curve follows the scaling until the energy error from the photon truncation does not reach roughly 10^{-6} , which would be roughly the expected accuracy of a calculation with

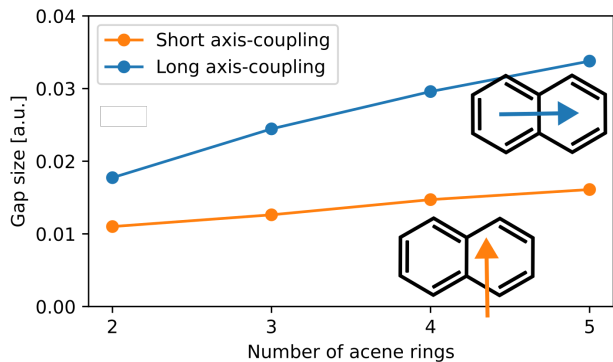


FIG. 8: Energetic splitting of the polaritonic states for different numbers of acene rings at a fixed coupling strength of $|\lambda| = 0.05$ a.u.. We compare two different possible orientations of the coupling vector.

a fixed truncation error of 10^{-6} . The convergence does not differ very significantly between the photon number and coherent basis formulations, however, the coherent formulation has the advantage of being translationally invariant, which in the photon number basis does not hold for charged molecules, unless we include enough photons in the calculation to saturate the wave function.^{18,26,52} On the other hand, the coherent state formulation uses the QED-RHF orbitals, which change with the coupling strength, and requires selecting an active space for every coupling vector separately, unlike with canonical RHF orbitals.

One advantage of the DMRG method we would like to stress is that the extra photons in the basis, which do not contribute to the wave function, are removed in the renormalization procedure, and thus mean a very small extra computational cost. This is in sharp contrast with QED-CASCI, where every extra photon inevitably means an increase in the Hamiltonian matrix size. To demonstrate this, in Figure 5 we show the maximal bond dimension for DBSS for each number of photons. There we can clearly see that increasing the number of photons after saturating the wave function has no effect on the total number of renormalized basis states, even when going to the extreme limit of allowing up to 100 photons.

To explicitly show the polaritonic splitting of the S_1 excited state of naphthalene, in Figure 6 we plot the dependence of excitation energies on the coupling strength. We find that, except for the split polaritonic state, the other states are affected by the interaction with the field equally, and thus the energy difference stays constant over the range. The split polaritonic state is then lowered in energy with respect to the other states, which can lead to states crossing, as can be seen for the S_1 and T_2 states in this case. The primary determinantal contributions to the resulting polaritonic state of naphthalene for $\lambda = 0.05$ a.u., with absolute CI coefficients greater than 0.01, are

$$\begin{aligned}
 |\Psi\rangle = & -0.883 |\text{HF det.}\rangle |1\omega\rangle + 0.119 |H-1 \rightarrow L\rangle |0\omega\rangle \\
 & + 0.119 |\overline{H-1} \rightarrow \overline{L}\rangle |0\omega\rangle + -0.116 |H \rightarrow L+1\rangle |0\omega\rangle \\
 & + -0.116 |\overline{H} \rightarrow \overline{L+1}\rangle |0\omega\rangle + 0.105 |H, \overline{H} \rightarrow L, \overline{L}\rangle |1\omega\rangle,
 \end{aligned}
 \tag{32}$$

where H and L denote the highest occupied molecular orbital (HOMO) and the lowest unoccupied molecular orbital (LUMO).

Similarly, we show the value of the polaritonic splitting of pentacene in Figure 7. Although the polaritonic splitting increases with the number of aromatic rings, due to the larger $S_1 - T_2$ gap, the state inversion occurs at higher coupling strengths.

By plotting the splitting value for a fixed coupling strength of $|\lambda| = 0.05$ a.u. in Figure 8, we observe a remarkable linear increase with the number of rings, despite the underlying complexity of the processes involved. This trend, which is more pronounced for the coupling oriented in plane along the long axis, highlights the influence of molecular structure on polaritonic behavior and suggests potential avenues for tuning the properties of polycyclic aromatic hydrocarbons through molecular design.

V. CONCLUSIONS

In conclusion, we have developed a novel method for cavity-QED calculations utilizing the DMRG algorithm, which facilitates near exact CASCI calculations with significantly larger active spaces than traditional canonical-CASCI method. This approach is particularly suitable for systems exhibiting strong correlation effects between electronic and photonic degrees of freedom. We have demonstrated the method's capabilities on the n -oligoacenes series, with n ranging from 2 to 5, successfully managing up to 22 fully correlated π orbitals in pentacene. Our numerical results indicate that employing a split-localized coherent state basis yields fastest convergence towards the exact results. Additionally, we have shown that in the acenes series, the polaritonic splitting increases almost linearly with the number of aromatic rings, highlighting the influence of molecular structure on polaritonic behaviour.

ACKNOWLEDGMENT

We acknowledge financial support from the Czech Science Foundation (grant no. 23-05486S), the Charles University Grant Agency (Grant No. 218222), the Ministry of Education, Youth and Sports of the Czech Republic through the e-INFRA CZ (ID:90254), the Advanced Multiscale Materials for Key Enabling Technologies project, supported by the Ministry of Education, Youth, and Sports of the Czech Republic. Project No. CZ.02.01.01/00/22_008/0004558, Co-funded by the European Union. JJF, NV, and NG acknowledge support from the Center for Many-Body Methods, Spectroscopies, and Dynamics for Molecular Polaritonic Systems (MAPOL) under

FWP 79715, which is funded as part of the Computational Chemical Sciences (CCS) program by the U.S. Department of Energy, Office of Science, Office of Basic Energy Sciences, Division of Chemical Sciences, Geosciences and Biosciences at Pacific Northwest National Laboratory (PNNL). PNNL is a multi-program national laboratory operated by Battelle Memorial Institute for the United States Department of Energy under DOE contract number DE-AC05-76RL1830. JJF gratefully acknowledges the NSF CAREER Award CHE-2043215.

REFERENCES

- F. Bernardot, P. Nussenzeig, M. Brune, J. M. Raimond, and S. Haroche, "Vacuum rabi splitting observed on a microscopic atomic sample in a microwave cavity," *Europhysics Letters* **17**, 33 (1992).
- P. Nussenzeig, F. Bernardot, M. Brune, J. Hare, J. M. Raimond, S. Haroche, and W. Gawlik, "Preparation of high-principal-quantum-number "circular" states of rubidium," *Phys. Rev. A* **48**, 3991–3994 (1993).
- R. Chikkaraddy, B. De Nijs, F. Benz, S. J. Barrow, O. A. Scherman, E. Rosta, A. Demetriadou, P. Fox, O. Hess, and J. J. Baumberg, "Single-molecule strong coupling at room temperature in plasmonic nanocavities," *Nature* **535**, 127–130 (2016).
- J. A. Hutchison, T. Schwartz, C. Genet, E. Devaux, and T. W. Ebbesen, "Modifying chemical landscapes by coupling to vacuum fields," *Angew. Chem., Int. Ed.* **51**, 1592 (2012).
- A. Thomas, "Ground state chemical reactivity under vibrational strong coupling to the vacuum electromagnetic field," *Angew. Chem., Int. Ed.* **55**, 11462 (2016).
- T. W. Ebbesen, A. Rubio, and G. D. Scholes, "Introduction: Polaritonic chemistry," *Chemical Reviews* **123**, 12037–12038 (2023), pMID: 37936399, <https://doi.org/10.1021/acs.chemrev.3c00637>.
- K. Hirai, J. A. Hutchison, and H. Uji-i, "Molecular chemistry in cavity strong coupling," *Chemical Reviews* **123**, 8099–8126 (2023).
- F. Pavošević, R. L. Smith, and A. Rubio, "Cavity click chemistry: Cavity-catalyzed azide–alkyne cycloaddition," *The Journal of Physical Chemistry A* **127**, 10184–10188 (2023), pMID: 37992280, <https://doi.org/10.1021/acs.jpca.3c06285>.
- M. Ruggenthaler, F. Mackenroth, and D. Bauer, "Time-dependent Kohn-Sham approach to quantum electrodynamics," *Phys. Rev. A* **84**, 042107 (2011).
- M. Ruggenthaler, J. Flick, C. Pellegrini, H. Appel, I. V. Tokatly, and A. Rubio, "Quantum-electrodynamical density-functional theory: Bridging quantum optics and electronic-structure theory," *Phys. Rev. A* **90**, 012508 (2014).
- C. Pellegrini, J. Flick, I. V. Tokatly, H. Appel, and A. Rubio, "Optimized effective potential for quantum electrodynamical time-dependent density functional theory," *Phys. Rev. Lett.* **115**, 093001 (2015).
- J. Flick, C. Schäfer, M. Ruggenthaler, H. Appel, and A. Rubio, "Ab initio optimized effective potentials for real molecules in optical cavities: Photon contributions to the molecular ground state," *ACS Photonics* **5**, 992–1005 (2018).
- R. Jestädt, M. Ruggenthaler, M. J. T. Oliveira, A. Rubio, and H. Appel, "Light-matter interactions within the ehrenfest–maxwell–pauli–kohn–sham framework: fundamentals, implementation, and nano-optical applications," *Advances in Physics* **68**, 225–333 (2019).
- J. Flick and P. Narang, "Ab initio polaritonic potential-energy surfaces for excited-state nanophotonics and polaritonic chemistry," *J. Chem. Phys.* **153**, 094116 (2020).
- M. Ruggenthaler, D. Sidler, and A. Rubio, "Understanding polaritonic chemistry from ab initio quantum electrodynamics," *Chem. Rev.* **123**, 11191–11229 (2023).
- N. Vu, G. M. McLeod, K. Hanson, and A. E. I. DePrince, "Enhanced diastereocontrol via strong light–matter interactions in an optical cavity," *J. Phys. Chem. A* **126**, 9303–9312 (2022).
- F. Pavošević and A. Rubio, "Wavefunction embedding for molecular polaritons," *J. Chem. Phys.* **157**, 094101 (2022).
- M. D. Liebenthal, N. Vu, and A. E. DePrince III, "Assessing the effects of orbital relaxation and the coherent-state transformation in quantum electrodynamics density functional and coupled-cluster theories," *J. Phys. Chem. A* **127**, 5264–5275 (2023).
- I. V. Tokatly, "Time-dependent density functional theory for many-electron systems interacting with cavity photons," *Phys. Rev. Lett.* **110**, 233001 (2013).
- J. Flick, M. Ruggenthaler, H. Appel, and A. Rubio, "Atoms and molecules in cavities, from weak to strong coupling in quantum-electrodynamics (QED) chemistry," *Proc. Natl. Acad. Sci. USA* **114**, 3026–3034 (2017).
- I. V. Tokatly, "Conserving approximations in cavity quantum electrodynamics: Implications for density functional theory of electron-photon systems," *Phys. Rev. B* **98**, 235123 (2018).
- J. Malave, A. Ahrens, D. Pitagora, C. Covington, and K. Varga, "Real-space, real-time approach to quantum-electrodynamical time-dependent density functional theory," *J. Chem. Phys.* **157**, 194106 (2022).
- J. Yang, Q. Ou, Z. Pei, H. Wang, B. Weng, Z. Shuai, K. Mullen, and Y. Shao, "Quantum-electrodynamical time-dependent density functional theory within gaussian atomic basis," *J. Chem. Phys.* **155**, 064107 (2021).
- J. Yang, Z. Pei, E. C. Leon, C. Wickizer, B. Weng, Y. Mao, Q. Ou, and Y. Shao, "Cavity quantum-electrodynamical time-dependent density functional theory within Gaussian atomic basis. II. Analytic energy gradient," *J. Chem. Phys.* **156**, 124104 (2022).
- J. McTague and J. J. Foley IV, "Non-hermitian cavity quantum electrodynamics—configuration interaction singles approach for polaritonic structure with ab initio molecular hamiltonians," *J. Chem. Phys.* **156**, 154103 (2022).
- N. Vu, D. Mejia-Rodriguez, N. P. Bauman, A. Panyala, E. Mutlu, N. Govind, and J. J. I. Foley, "Cavity quantum electrodynamics complete active space configuration interaction theory," *Journal of Chemical Theory and Computation* **20**, 1214–1227 (2024), pMID: 38291561, <https://doi.org/10.1021/acs.jctc.3c01207>.
- M. Bauer and A. Dreuw, "Perturbation theoretical approaches to strong light–matter coupling in ground and excited electronic states for the description of molecular polaritons," *J. Chem. Phys.* **158**, 124128 (2023), https://pubs.aip.org/aip/jcp/article-pdf/doi/10.1063/5.0142403/16794111/124128_1_online.pdf.
- Z.-H. Cui, A. Mandal, and D. R. Reichman, "Variational lang–firsov approach plus møller–plesset perturbation theory with applications to ab initio polariton chemistry," *Journal of Chemical Theory and Computation* **20**, 1143–1156 (2024), pMID: 38300885, <https://doi.org/10.1021/acs.jctc.3c01166>.
- T. S. Haugland, C. Schäfer, E. Ronca, A. Rubio, and H. Koch, "Intermolecular interactions in optical cavities: An ab initio qed study," *J. Chem. Phys.* **154**, 094113 (2021).
- U. Mordovina, C. Bungey, H. Appel, P. J. Knowles, A. Rubio, and F. R. Manby, "Polaritonic coupled-cluster theory," *Physical Reviews Research* **2**, 023262 (2020).
- A. E. DePrince, "Cavity-modulated ionization potentials and electron affinities from quantum electrodynamics coupled-cluster theory," *J. Chem. Phys.* **154**, 094112 (2021).
- J. D. Mallory and A. E. DePrince, "Reduced-density-matrix-based ab initio cavity quantum electrodynamics," *Phys. Rev. A* **106**, 053710 (2022).
- B. M. Weight, S. Tretiak, and Y. Zhang, "Diffusion quantum monte carlo approach to the polaritonic ground state," *Phys. Rev. A* **109**, 032804 (2024).
- N. M. Tubman, C. D. Freeman, D. S. Levine, D. Hait, M. Head-Gordon, and K. B. Whaley, "Modern approaches to exact diagonalization and selected configuration interaction with the adaptive sampling ci method," *Journal of Chemical Theory and Computation* **16**, 2139–2159 (2020).
- Y. Garniron, A. Scemama, E. Giner, M. Caffarel, and P.-F. Loos, "Selected configuration interaction dressed by perturbation," *The Journal of Chemical Physics* **149** (2018), 10.1063/1.5044503.
- W. Liu and M. R. Hoffmann, "ici: Iterative ci toward full ci," *Journal of Chemical Theory and Computation* **12**, 1169–1178 (2016).
- S. Sharma, A. A. Holmes, G. Jeanmairet, A. Alavi, and C. J. Umrigar, "Semistochastic heat-bath configuration interaction method: Selected configuration interaction with semistochastic perturbation theory," *Journal of Chemical Theory and Computation* **13**, 1595–1604 (2017).

- ³⁸K. Guther, R. J. Anderson, N. S. Blunt, N. A. Bogdanov, D. Cleland, N. Dattani, W. Dobrautz, K. Ghanem, P. Jeszenszki, N. Liebermann, G. L. Manni, A. Y. Lozovoi, H. Luo, D. Ma, F. Merz, C. Overy, M. Ramp, P. K. Samanta, L. R. Schwarz, J. J. Shepherd, S. D. Smart, E. Vitale, O. Weser, G. H. Booth, and A. Alavi, "Neci: N-electron configuration interaction with an emphasis on state-of-the-art stochastic methods," *The Journal of Chemical Physics* **153** (2020), 10.1063/5.0005754.
- ³⁹G. K.-L. Chan and S. Sharma, "The density matrix renormalization group in quantum chemistry," *Annu. Rev. Phys. Chem.* **62**, 465–481 (2011).
- ⁴⁰S. Szalay, M. Pfeffer, V. Murg, G. Barcza, F. Verstraete, R. Schneider, and Örs Legeza, "Tensor product methods and entanglement optimization for ab initio quantum chemistry," *Int. J. Quant. Chem.* **115**, 1342–1391 (2015).
- ⁴¹A. Baiardi and M. Reiher, "The density matrix renormalization group in chemistry and molecular physics: Recent developments and new challenges," *J. Chem. Phys.* **152**, 040903 (2020).
- ⁴²J. Brabec, J. Brandejs, K. Kowalski, S. Xantheas, Ö. Legeza, and L. Veis, "Massively parallel quantum chemical density matrix renormalization group method," *J. Comput. Chem.* **42**, 534–544 (2021).
- ⁴³S. R. White, "Density matrix formulation for quantum renormalization groups," *Phys. Rev. Lett.* **69**, 2863–2866 (1992).
- ⁴⁴K. Lopata, R. Reslan, M. Kowalska, D. Neuhauser, N. Govind, and K. Kowalski, "Excited-state studies of polyacenes: A comparative picture using eomccsd, cr-eomccsd(t), range-separated (lr/rt)-tdtft, td-pm3, and td-zindo," *Journal of chemical theory and computation* **7**, 3686–3693 (2011).
- ⁴⁵S. R. White, "Density-matrix algorithms for quantum renormalization groups," *Phys. Rev. B* **48**, 10345–10356 (1993).
- ⁴⁶U. Schollwöck, "The density-matrix renormalization group in the age of matrix product states," *Ann. Phys.* **326**, 96–192 (2011).
- ⁴⁷E. R. Davidson, "The iterative calculation of a few of the lowest eigenvalues and corresponding eigenvectors of real-symmetric matrices," *J. Comput. Phys.* **17**, 87–94 (1975).
- ⁴⁸T. Xiang, "Density-matrix renormalization-group method in momentum space," *Physical Review B* **53**, R10445–R10448 (1996).
- ⁴⁹A. Muolo, A. Baiardi, R. Feldmann, and M. Reiher, "Nuclear-electronic all-particle density matrix renormalization group," *The Journal of Chemical Physics* **152** (2020), 10.1063/5.0007166.
- ⁵⁰R. Feldmann, A. Muolo, A. Baiardi, and M. Reiher, "Quantum proton effects from density matrix renormalization group calculations," *Journal of Chemical Theory and Computation* **18**, 234–250 (2022).
- ⁵¹J. R. Klauder and E. C. G. Sudarshan, *Fundamentals of quantum optics* (W. A. Benjamin, Inc, New York, 1968).
- ⁵²J. J. Foley IV, J. McTague, and A. E. DePrince III, "Ab initio methods for polariton chemistry," *Chem. Phys. Rev* **4**, 041301 (2023).
- ⁵³O. Legeza and J. Sólyom, "Optimizing the density-matrix renormalization group method using quantum information entropy," *Phys. Rev. B* **68** (2003).
- ⁵⁴H. R. Larsson, H. Zhai, K. Gunst, and G. K.-L. Chan, "Matrix product states with large sites," *Journal of Chemical Theory and Computation* **18**, 749–762 (2022), pMID: 35060382, <https://doi.org/10.1021/acs.jctc.1c00957>.
- ⁵⁵G. Barcza, M. A. Werner, G. Záránd, A. Pershin, Z. Benedek, O. Legeza, and T. Szilvási, "Toward large-scale restricted active space calculations inspired by the schmidt decomposition," *The Journal of Physical Chemistry A* **126**, 9709–9718 (2022), pMID: 36520596, <https://doi.org/10.1021/acs.jpca.2c05952>.
- ⁵⁶R. Feldmann, A. Muolo, A. Baiardi, and M. Reiher, "Quantum proton effects from density matrix renormalization group calculations," *Journal of Chemical Theory and Computation* **18**, 234–250 (2022), pMID: 34978441, <https://doi.org/10.1021/acs.jctc.1c00913>.
- ⁵⁷E. Jeckelmann and S. R. White, "Application of the dmrg technique to the holstein model," in *APS March Meeting Abstracts* (1996) pp. O13–10.
- ⁵⁸E. Jeckelmann and S. R. White, "Density-matrix renormalization-group study of the polaron problem in the holstein model," *Physical Review B* **57**, 6376 (1998).
- ⁵⁹M. Tezuka, R. Arita, and H. Aoki, "A dmrg study of correlation functions in the holstein–hubbard model," *Physica B: Condensed Matter* **359**, 708–710 (2005).
- ⁶⁰H. Zhai, H. R. Larsson, S. Lee, Z.-H. Cui, T. Zhu, C. Sun, L. Peng, R. Peng, K. Liao, J. Tölle, *et al.*, "Block2: A comprehensive open source framework to develop and apply state-of-the-art dmrg algorithms in electronic structure and beyond," *The Journal of Chemical Physics* **159** (2023).
- ⁶¹P. Beran, M. Matoušek, M. Hapka, K. Pernal, and L. Veis, "Density matrix renormalization group with dynamical correlation via adiabatic connection," *Journal of Chemical Theory and Computation* **17**, 7575–7585 (2021), pMID: 34762423, <https://doi.org/10.1021/acs.jctc.1c00896>.
- ⁶²T. H. Dunning, "Gaussian basis sets for use in correlated molecular calculations. I. The atoms boron through neon and hydrogen," *J. Chem. Phys.* **90**, 1007–1023 (1989).
- ⁶³R. Olivares-Amaya, W. Hu, N. Nakatani, S. Sharma, J. Yang, and G. K.-L. Chan, "The ab-initio density matrix renormalization group in practice," *J. Chem. Phys.* **142**, 034102 (2015).
- ⁶⁴M. Fiedler, "Algebraic connectivity of graphs," *Czechoslovak mathematical journal* **23**, 298–305 (1973).
- ⁶⁵M. Fiedler, "Eigenvectors of acyclic matrices," *Czechoslovak Mathematical Journal* **25**, 607–618 (1975).
- ⁶⁶G. Barcza, O. Legeza, K. H. Marti, and M. Reiher, "Quantum-information analysis of electronic states of different molecular structures," *Phys. Rev. A* **83**, 012508 (2011).
- ⁶⁷Ö. Legeza, J. Röder, and B. Hess, "Controlling the accuracy of the density-matrix renormalization-group method: The dynamical block state selection approach," *Phys. Rev. B* **67**, 125114 (2003).
- ⁶⁸S. R. White and R. L. Martin, "Ab initio quantum chemistry using the density matrix renormalization group," *The Journal of Chemical Physics* **110**, 4127–4130 (1999), https://pubs.aip.org/aip/jcp/article-pdf/110/9/4127/19023329/4127_1_online.pdf.
- ⁶⁹G. K.-L. Chan and M. Head-Gordon, "Highly correlated calculations with a polynomial cost algorithm: A study of the density matrix renormalization group," *The Journal of chemical physics* **116**, 4462–4476 (2002).